



Submitted to

---

**International Europhysics Conference on High Energy Physics, EPS03**, July 17-23, 2003, Aachen  
(Abstract **096** Parallel Session **4**)

**XXI International Symposium on Lepton and Photon Interactions, LP03**, August 11-16, 2003, Fermilab

---

[www-h1.desy.de/h1/www/publications/conf/conf\\_list.html](http://www-h1.desy.de/h1/www/publications/conf/conf_list.html)

## **Measurement of Inclusive $D$ -meson Production in Deep Inelastic Scattering at HERA**

H1 Collaboration

### **Abstract**

The inclusive production of charmed mesons in deep inelastic scattering is studied with the H1 detector at HERA. Inclusive production cross sections are measured for the vector  $D^{*+}$  and for the pseudoscalar mesons  $D^0$ ,  $D_S$  and, for the first time at HERA, also  $D^+$ . The finite lifetimes of 0.4 to 1 ps for the pseudoscalar mesons lead to a separation of their production and decay vertices, which is exploited to distinguish signal and background processes and to substantially improve the signal qualities. Differential distributions are measured for the  $D^+$  and  $D^0$  mesons and compared with predictions based on LO Monte Carlo simulations.

The measured production cross sections are used to test the isospin invariance of the fragmentation process and to extract the strangeness suppression factor  $\gamma_s$  and the fraction  $P_V$  of  $D$  mesons produced in a vector state. The results are compared with values measured e.g. at  $e^+e^-$  colliders and allow tests of the assumed universality of the charm fragmentation process.

# 1 Introduction

The production of heavy quarks in electron-proton interactions proceeds, in QCD, almost exclusively via photon-gluon fusion, where a photon coupling to the incoming electron interacts with a gluon in the proton to form a quark-antiquark pair. This holds both for deep inelastic scattering (DIS) and for photoproduction, where the exchanged photon is almost real. Differential charm production cross section measurements [1–3] in the range of experimental acceptance were found to be reasonably well reproduced by a description based on perturbative QCD (pQCD) done at Leading Order (LO) and at Next to Leading Order (NLO) [4]. However, all these calculations are performed at the parton level, and the conversion of the parton to hadrons – the hadronisation process itself – is modelled by means of fragmentation functions:

$$d\sigma_h(p) = \int d\hat{\sigma}(p/z, \mu) \cdot D_h^q(z, \mu) dz. \quad (1)$$

Here  $d\hat{\sigma}(p/z, \mu)$  describes the partonic cross section and  $\mu$  the factorization scale. The fragmentation function  $D_h^q(z, \mu)$  describes the probability for a quark  $q$  with momentum  $p$  to produce a hadron  $h$  with momentum fraction  $z$ , and contains both a perturbative part (following an evolution in  $\mu$  within the DGLAP formalism) and a non-perturbative part  $D_{NP}(z)$ , which is conventionally assumed to be universal. Under the assumption of factorisation and universality, this  $D_{NP}(z)$  is tuned at  $e^+e^-$  colliders to hadron decay spectra and then applied to hadronisation processes at HERA.

It has been argued by Nason *et al.* [5,6], however, that these assumptions may not hold, and that in fact different processes may be sensitive to different aspects of fragmentation. Thus it is necessary to test the hypotheses of universality and factorisation in many different processes.

This paper describes one way of doing this, namely through the comparison of the production rates of the various different charmed meson states. These  $D$ -meson states are identified by means of a lifetime tag, i.e. by measuring the decay length distributions.

The paper describes a measurement of the H1 Collaboration and is organized in four sections: first the established measurement of the  $D^*$  production cross section is repeated using only the central tracking chamber (CJC) information and shown to be consistent with previous publications. Next, confidence in the understanding of the new H1 silicon tracker (CST), used subsequently for the lifetime tagging method, is established by showing the high level of agreement with which the MC simulations describe the data. For this purpose “tagged  $D^0$  mesons” are used; these are those  $D^0$ s unambiguously identified, using the  $\Delta m$  method, as originating from a  $D^*$  decay. Then the determination of the cross sections of the different new decay channels, based on lifetime tagging, is presented. Finally, because the results of the different channels are extracted within the same visible kinematic regime, they allow the determination of ratios sensitive to fragmentation.

## 2 Experimental Aspects and Data Analysis

### 2.1 Detector, Kinematics and Simulation

The data have been collected with the H1 detector at HERA and correspond in total to integrated luminosities of  $(47.8 \pm 0.7) \text{ pb}^{-1}$  of  $e^+p$  interactions at  $\sqrt{s} = 318 \text{ GeV}$ . The charmed mesons

are detected through their decay products, in particular  $D^+ \rightarrow K^- \pi^+ \pi^+$ ,  $D^0 \rightarrow K^- \pi^+$ ,  $D_s^+ \rightarrow \phi \pi^+ \rightarrow (K^+ K^-) \pi^+$  and  $D^{*+} \rightarrow D^0 \pi^+ \rightarrow (K^- \pi^+) \pi^+$ .<sup>1</sup>

The H1 detector and its trigger capabilities have been described in detail elsewhere [7]. Charged particles are measured by a set of tracking devices: two cylindrical jet drift chambers (CJC) [8, 9], mounted concentrically around the beam-line inside a homogeneous magnetic field of 1.15 T, yielding particle charge and momentum from the track curvature in the polar angular range of  $20^\circ < \theta < 160^\circ$ , where  $\theta$  is measured using the CJC and two polygonal  $z$  drift chambers and is defined with respect to the incident proton beam direction. These central tracking devices are complemented by the central silicon tracker (CST) [10] with two layers at 57.5 mm and 97.5 mm radii. The CST is centred at the nominal interaction point and has an active length of 356 mm in the  $z$ -direction. Its intrinsic spatial resolution is  $12 \mu\text{m}$  in  $r\phi$  and  $22 \mu\text{m}$  in  $z$ , and serves for the vertex separation measurement of the long lived particles. One double layer of cylindrical multi-wire proportional chambers (MWPC) [11] with pad readout for triggering purposes is positioned between the CST and the CJC, and another between the two jet chambers. The backward region ( $153^\circ < \theta < 177.8^\circ$ ) of H1 is equipped with a lead scintillator ‘‘Spaghetti’’ calorimeter (SpaCal) [12], which is optimized for the detection of the scattered electron in the DIS kinematic range under consideration here and provides time-of-flight functionality for trigger purposes. It consists of an electromagnetic and a more coarsely segmented hadronic section. A four-layer drift chamber (BDC) [13] mounted in front of the SpaCal is used to reject neutral particle background.

The events used here have been triggered by an electromagnetic cluster in the SpaCal of at least 6.0 GeV energy in coincidence with a charged track signal from the MWPC and central drift chamber trigger.

## 2.2 Event Selection and Reconstruction

The analysis covers the kinematic regime of  $2 < Q^2 < 100 \text{ GeV}^2$  and  $0.05 < y < 0.7$ , where the scattered electron is used to determine the event kinematic quantities. The identification of electrons is similar to the procedure used in the inclusive structure function measurement [14]. Scattered electrons are identified as clusters in the SpaCal with energy  $E_{e'} > 8 \text{ GeV}$ , with a cluster radius  $< 3.5 \text{ cm}$  consistent with electromagnetic energy deposition, and with a cluster centre matched by a charged track candidate in the BDC within 2.5 cm. The scattering angle is required to be  $153^\circ < \theta_{e'} < 177^\circ$ .

The DIS kinematic variables are reconstructed using the ‘‘electron ( $e$ )’’ method [15], where

$$Q^2 = 4E_e E_{e'} \cos^2 \frac{\theta_{e'}}{2}, \text{ and } y_e = 1 - (E_{e'}/E_e) \sin^2(\theta_{e'}/2) \quad (2)$$

with  $E_e, E_{e'}$  denoting the energies of the incoming and scattered electron respectively. The results obtained with the  $e$  method have been checked with another (‘‘ $\Sigma'$ ’’ [15]) method and are found to be in very good agreement. The absolute energy scale of the SpaCal is known to a precision of  $\pm 4\%$ .

---

<sup>1</sup>Hereafter, the charge conjugate states are always implicitly included.

## 2.3 Signal Determination

The reconstruction of the various  $D$  mesons proceeds as follows: charged particle tracks passing some standard quality cuts and fulfilling transverse momentum cuts as listed in table 1 are combined, and the resulting combinations loosely tested for compatibility with possible  $D$  decay hypotheses. No particle identification is applied at any stage. Assuming each track to be appropriately either a kaon or a pion, the tracks of correct sign charges are combined and taken to determine the number of signal events in each channel as follows:

a)  $D^+ \rightarrow K^- \pi^+ \pi^+$ : the 3-particle invariant mass distribution  $m(K\pi\pi)$  is directly fitted by a Gaussian signal and a linear background shape (see fig. 1).

b)  $D^0 \rightarrow K^- \pi^+$ : the signal is directly extracted from a fit of the  $K^- \pi^+$  candidate invariant mass distribution  $m(K\pi)$  with a function composed of a Gaussian signal  $G_{sig}$ , an exponential combinatorial background  $B$  and a wrong-charge combination contribution  $G_{wc}$ , approximated by a broad Gaussian. The mean position and the width of  $G_{wc}$  as well as the normalisation ratio of  $G_{sig}$  to  $G_{wc}$  have been determined from the MC simulation and subsequently kept fixed in the fit (see fig. 2).

c)  $D_s^+ \rightarrow \phi \pi^+ \rightarrow (K^+ K^-) \pi^+$ : because the  $D_s$  decays through the intermediate vector-meson  $\phi$  resonance, it lends itself to further specific kinematic constraints. In particular, the two particle combination  $m(K^+ K^-)$  is required to lie within  $2\sigma$  of the nominal  $\phi$  mass (i.e. within 11 MeV of 1020 MeV). Furthermore, the angular distribution of the  $K$ -meson flight direction transformed into the  $\phi$  rest frame (the helicity angle  $\theta^*$ ) follows a  $\cos^2 \theta^*$  shape. To reduce combinatorial background,  $|\cos \theta^*| > 0.4$  is required. Both the  $D_s$  and the  $\phi$  distributions are shown in fig. 3.

d)  $D^{*+} \rightarrow D^0 \pi^+ \rightarrow (K^- \pi^+) \pi^+$ : the well-known  $\Delta m$ -tagging technique is applied [16]. For all candidate combinations lying within  $\pm 3\sigma$  of the nominal value of  $\Delta m$ , the invariant mass  $m(K\pi)$  distribution is fitted with a Gaussian signal and an exponential background shape, and  $N_{D^*}$  thus determined (see fig. 4).  $D^0$  mesons from an identified  $D^{*+} \rightarrow D^0 \pi^+ \rightarrow (K^- \pi^+) \pi^+$  chain will be referred to as tagged  $D^0$ s.

In the case of  $D$ -meson differential distributions, the inclusive data sample is divided into bins and the number of signal events extracted in each bin separately. The position and width of the Gaussian signal shape are fixed to the values found in the inclusive sample. The normalizations of the signal and the background are left as free parameters in the various fits. Other methods of determining the number of candidates have also been applied and the variation entered into the systematic error. Possible uncertainties due to assumptions about the background shapes have been estimated by changing the background shape (from linear to exponential), and are also taken into account in the systematic errors listed in table 4. Contributions to the signals due to other charm decays (so-called reflections) are estimated from Monte Carlo simulations to be at most 3%, and are included in the systematic errors.

## 2.4 Vertexing Issues

The finite lifetime of 0.4 to 1 ps of the  $D$  mesons leads to a spatial separation between their production (assumed to be the primary) and decay (secondary) vertices, which is measured in terms of the radial decay length  $l$  with error  $\sigma_l$ . Its significance  $S_l = l/\sigma_l$  constitutes one of

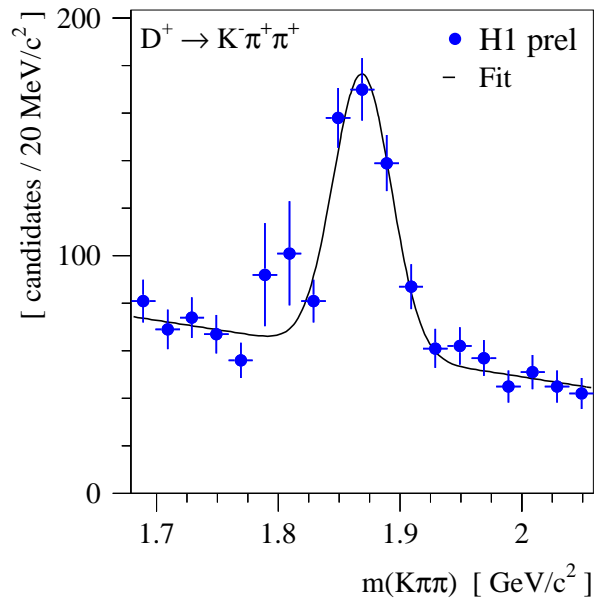


Figure 1: Invariant mass distribution  $m(K\pi\pi)$  of  $D^+$  candidates.

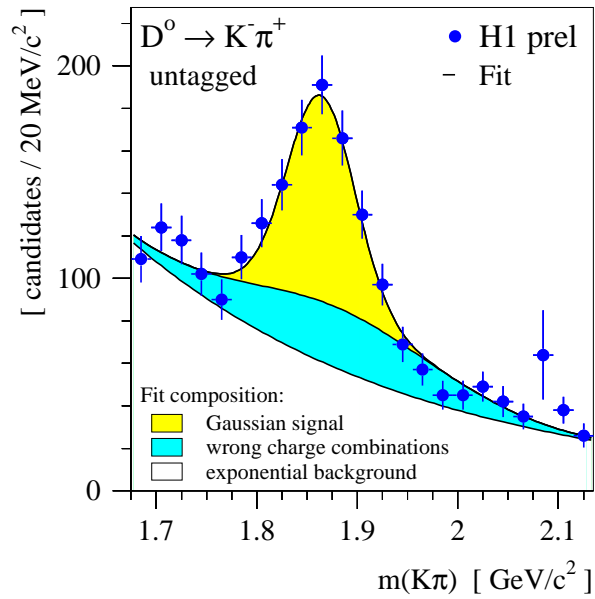


Figure 2: Invariant mass distribution  $m(K\pi)$  of  $D^0$  candidates. The decomposition of the data into the correct charge combination signal (light shading), the wrong charge combination (dark shading) and the exponential background is separately indicated.

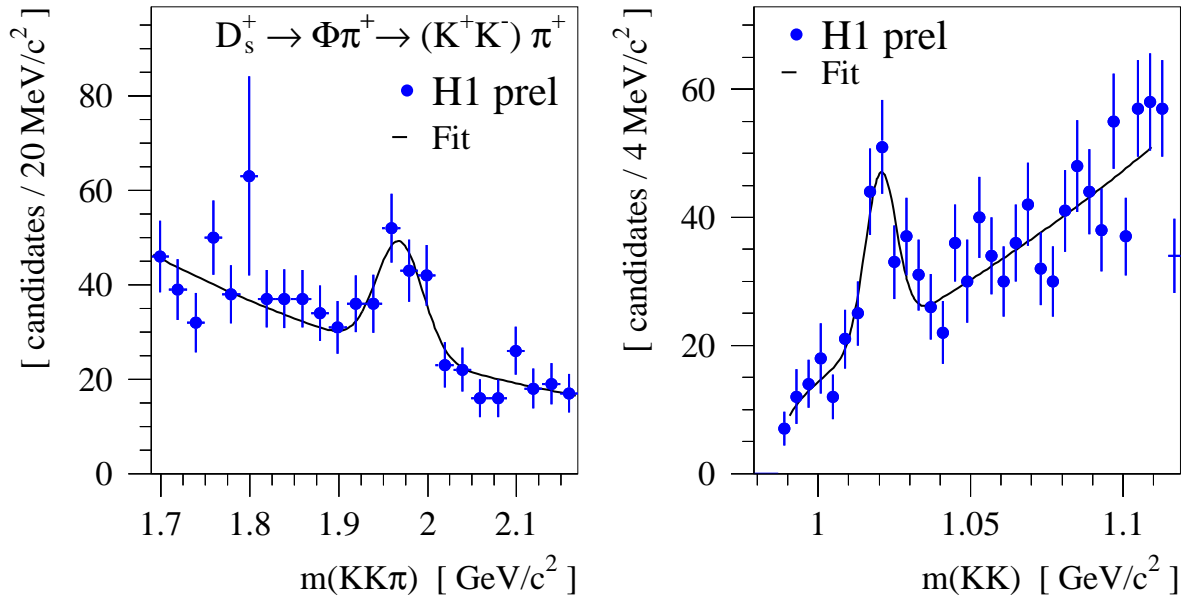


Figure 3: Invariant mass distributions  $m(KK\pi)$  of  $D_S$  candidates (left) and  $m(KK)$  of the intermediate  $\phi$ -resonance candidates (right).

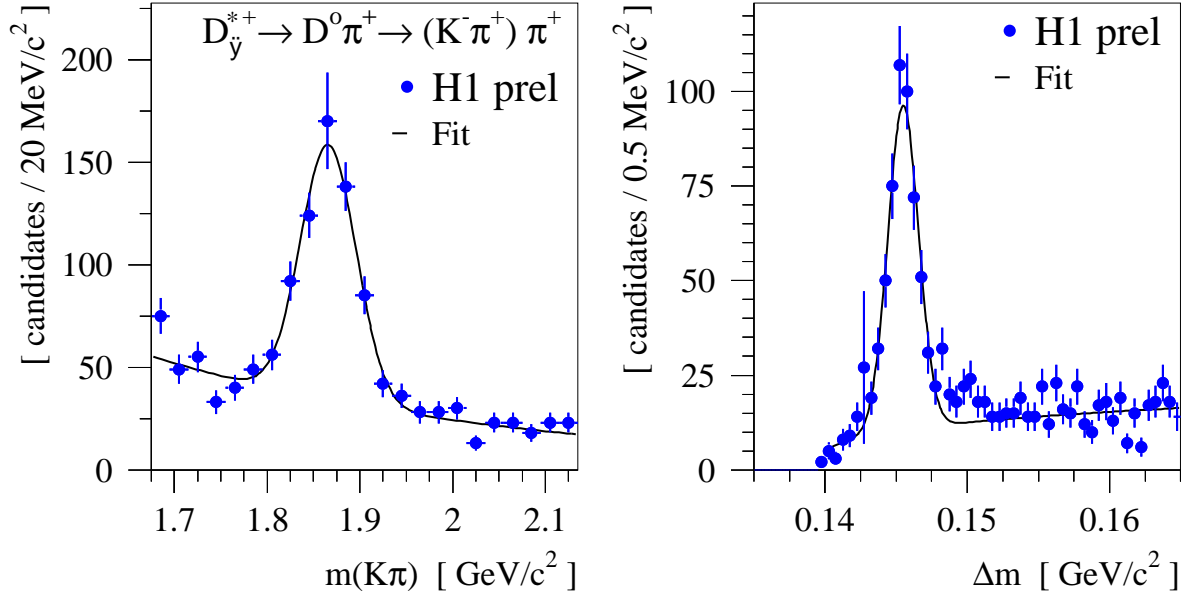


Figure 4:  $D^*$  candidate distributions: left:  $K\pi$  invariant mass after a  $3\sigma$  cut in  $\Delta m$ ; right: the  $\Delta m$  distribution after a  $2\sigma$  cut in  $m(K\pi)$  around the nominal value.

<b>Selection criteria</b>	$D^+$	$D^0$	$D_s^+$	$D^{*+}$
$\min p_t(K)$ [MeV/c]	500	800	400	250
$\min p_t(\pi)$ [MeV/c]	400	800	400	250
$\min p_t(\pi_s)$ [MeV/c]	-	-	-	140
$\min  \cos(\theta^*) $	-	-	0.4	-
$\theta_{track}$	[ 20°, 160° ]			
max decay length error $\sigma_l$	300 $\mu\text{m}$			
min fit probability $\mathcal{P}_{VF}$	0.05			
min decay length sig. $S_l = l/\sigma_l >$	5	3	2	1
min impact par. sig. ( $2 \times S_d >$ )	2.5	2	1	-1

Table 1: Selection criteria for the charged daughter tracks for each decay mode. The requirements on the vertexing parameters are also listed.

the most powerful quantities to distinguish long-lived hadrons from background events, which originate predominantly from random tracks from the primary vertex. The calculation of  $S_l$  depends on the understanding of the combination of CST and CJC information.

To obtain tracks with the desired precision, the well-established CJC tracks [8] are geometrically extrapolated into the CST. The closest CST hits available within a  $5\sigma$  search window are assigned to the tracks and these CJC-track / CST-hit combinations are then refitted. Each track can thus have up to 2 CST hits assigned.

Combinations of these CST-improved tracks (2 or 3 depending on the decay mode) are then fitted in the  $r\phi$  plane to a common secondary vertex under the assumption that the  $D$ -meson mother particle decayed into (2 or 3) daughter particles at this secondary vertex. A combination of tracks is taken if at least two of the tracks have an impact parameter  $d$  with significance  $S_d = d/\sigma_d$  larger than a minimal value. Of these tracks only one is allowed to have at most one CST hit missing. This effectively restricts the  $D$  mesons to lie in a polar angular range of typically  $25^\circ < \theta < 155^\circ$ . In the fit, the mother particle  $D$  is constrained to have originated from the primary vertex.

$D$ -meson decay candidates are selected by quality requirements on the vertexing, in particular on the probability of the vertex fit  $\mathcal{P}_{VF}$  and on the vertex separation significance  $S_l = l/\sigma_l$ . The cut values actually applied on  $\sigma_l$ ,  $\mathcal{P}_{VF}$ ,  $S_l$  and  $S_d$  are listed in table 1. The degree of improvement is demonstrated in fig. 5 in a comparison of the  $D^+$  signal before and after a cut on  $S_l$ .

The simulation of the silicon tracker CST has been scrutinized in detailed comparisons with data distributions by using among others tagged  $D^0$  events.

To indicate the level of understanding of the vertexing simulation, fig. 6a shows the measured decay length significance distribution  $S_l$  of tagged  $D^0$  candidates (solid dots). Separately shown is its fitted decomposition into a signal (hatched) and a background (shaded) contribution. The functional form of the signal distribution  $F_S$  is taken from the simulation, whereas the background shape  $F_B$  is extracted from the 250-MeV-wide sideband region in the  $m(K\pi)$  spectrum of the data. In the fit, only the normalisations of the signal and of the background are left as free parameters. The excellent  $\chi^2/ndf = 34/32$  indicates that the MC simulation describes the signal shape very well. Furthermore, the number of  $D^0$  candidates extracted by

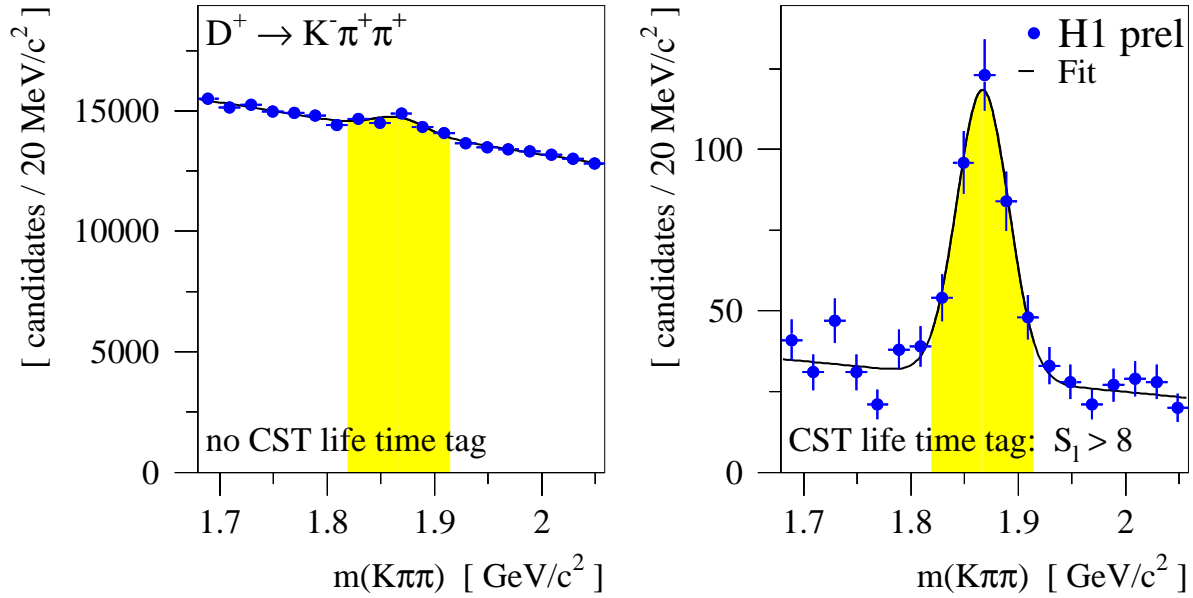


Figure 5: Comparison of the invariant mass distributions  $m(K\pi\pi)$  for  $D^+ \rightarrow K^-\pi^+\pi^+$  decay candidates (a) before and (b) after a cut on the decay length significance  $S_l = l/\sigma_l > 8$ . The background contribution is suppressed by  $\mathcal{O}(300)$  and the signal to background ratio is improved by a factor  $\mathcal{O}(50)$  when vertexing information measured with the H1 central silicon vertex detector CST is exploited.

means of the  $S_l$  fit is fully consistent within errors with the one determined from the fit of the invariant mass distribution  $m(K\pi)$ .

The efficiency  $\epsilon(S_l)$  as a function of the cut on  $S_l$  as measured in data (solid dots) is shown in fig. 6b to be very reasonably described by the MC simulation (open squares).

## 2.5 Acceptance and efficiency determination

A Monte Carlo simulation is used to determine the detector acceptance and the efficiency of the reconstruction and the selection cuts. Electroproduction events were generated in Leading Order with the AROMA 2.2 [17] program, combined with parton showering [18]. The hadronization step was performed according to the Lund string model, tuned to the world average fragmentation factors  $f_{w.a.}(c \rightarrow D)$ , which are dominated by the LEP results. The generated events were then processed by the H1 detector simulation program, and were subjected to the same reconstruction and analysis chain as the real data.

For the different decay channels  $D^+$ ,  $D^0$ ,  $D_S$  and  $D^*$ , the efficiencies and acceptances are given in table 2.

The dependence of the simulated acceptances and efficiencies on parameter choices made for the simulation (charm mass, parton density distributions, fragmentation parameters and QCD scales) was found to be less than  $\pm 2\%$  in all cases and is included in the theoretical systematic error.

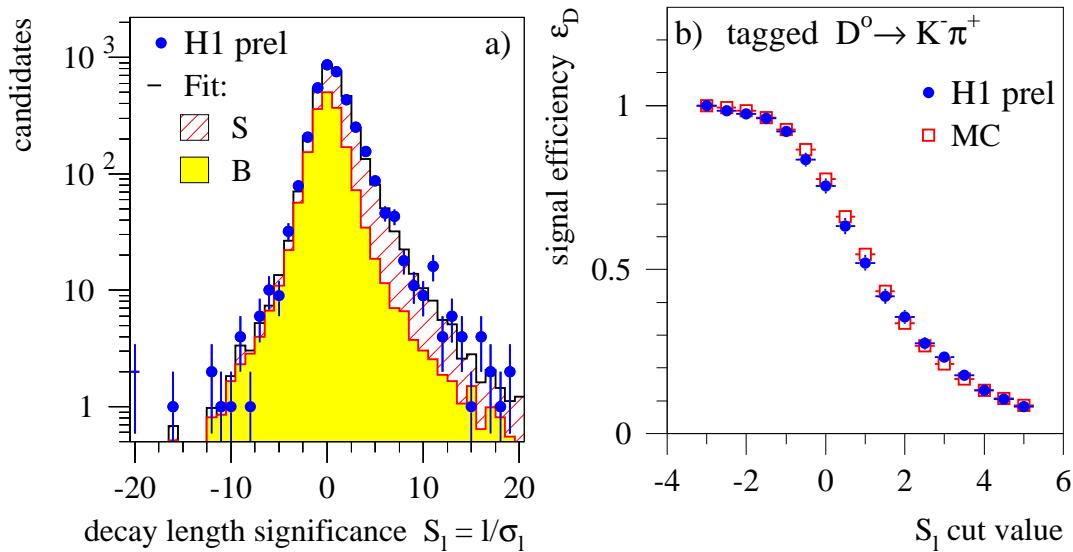


Figure 6: a) Distribution of the decay length significance  $S_l$  for data (solid dots), and the fitted decomposition into signal (hatched) and background (shaded) contributions. b) Efficiency as a function of the cut on the decay length significance  $S_l = l/\sigma_l$ ; the efficiency is defined as the number of fitted  $D^0$  mesons after applying the cut on  $S_l$  divided by the total number of  $D^0$  mesons without  $S_l$  cuts. Data (solid dots) are compared with the expectations from the simulation (open squares).

	$D^+$	$D^0$	$D_s^+$	$D^{*+}$
overall detector efficiency (%)	50.8	61.2	48.8	52.1
vertexing efficiency (%)	19.9	12.4	22.2	39.4
acceptance (%)	36.4	43.8	49.2	61.9

Table 2: Efficiency and acceptance values in (%) for the four meson states.

Contributions from  $b\bar{b}$  production, with subsequent decays of  $b$  flavoured hadrons into  $D$  mesons, have been calculated using the AROMA generator. No subtraction is made: the quoted  $D^*$  cross sections thus include any  $b$  contributions. A systematic error incorporates the change in efficiency brought about by a variation of the  $b\bar{b}$  contribution by  $\pm 30\%$  around the published  $b\bar{b}$  cross section [19], which shows an unexpectedly high excess over QCD expectation.

### 3 Results

#### 3.1 Production Cross Sections

The production cross sections are determined for all four decay channels for the identical visible kinematic range of  $2 \text{ GeV}^2 \leq Q^2 \leq 100 \text{ GeV}^2$ ,  $0.05 \leq y \leq 0.7$ ,  $p_t(D) \geq 2.5 \text{ GeV}/c$ ,  $|\eta(D)| \leq 1.5$ . Here  $\sigma_{vis}$  is defined as the sum of both particle and antiparticle meson states, and is given by

$$\sigma_{vis}(ep \rightarrow eDX) = \left\{ \sigma_{vis}(ep \rightarrow ec\bar{c}X) \cdot 2 \cdot f(c \rightarrow D) \right\}_{vis} + \left\{ \sigma_{vis}(ep \rightarrow eb\bar{b}X) \cdot 2 \cdot f(b \rightarrow D) \right\}_{vis}$$

where  $f(c \rightarrow D)$  and  $f(b \rightarrow D)$  are the charm and beauty fragmentation fractions into the respective  $D$  meson states. The factor of two corresponds to the fact that both  $c$  and  $\bar{c}$  may decay into the final state under consideration. The measured values of the visible cross sections for the four meson decay channels are summarized in table 3.

<b>Cross section</b>	$D^+$	$D^0$	$D_s^+$	$D^{*+}$
$\sigma_{vis}(ep \rightarrow eDX)$ (nb)	2.16	6.53	1.67	2.90
stat error on $\sigma_{vis}$	$\pm 0.19$	$\pm 0.49$	$\pm 0.41$	$\pm 0.20$
syst error on $\sigma_{vis}$	+0.46 -0.35	+1.06 -1.30	+0.54 -0.54	+0.58 -0.44
AROMA LO prediction $\sigma_{vis}$	2.45	5.54	1.15	2.61
uncertainty	$\pm 0.30$	$\pm 0.69$	$\pm 0.30$	$\pm 0.31$

Table 3: Inclusive charmed meson electroproduction cross sections for the four meson states in the visible kinematic range, defined by  $2 \leq Q^2 \leq 100 \text{ GeV}^2$ ,  $0.05 \leq y \leq 0.7$ ,  $p_t(D) \geq 2.5 \text{ GeV}/c$  and  $|\eta(D)| \leq 1.5$ .

### 3.2 Systematic Errors

The various contributions to the systematic errors on  $\sigma_{vis}$  are summarized in table 4. They are dominated by CJC tracking efficiency ( $^{+5}_{-1}$ %) per track) and by the vertexing uncertainty of 10%. A variation of the CST spatial resolution of up to 20% shows only a minor effect on  $\sigma_{vis}$  of order  $< 4\%$ . The SpaCal energy scale uncertainty is taken into account by a variation of  $\pm 4\%$ , and it contributes a change in  $\sigma_{vis}$  of  $(^{+5}_{-9})\%$ .

Included in the table is the uncertainty due to variations in the Monte Carlo acceptance, which itself is dominated by the charm mass variation ( $1.4 < m_c < 1.6 \text{ GeV}$ ) and the fragmentation uncertainties. Separately indicated is the error due to initial state radiation (ISR) corrections.

### 3.3 Comparison of Cross Sections with Predictions

The measured cross sections have been compared in detail with LO calculations. The corresponding predictions using the AROMA MC generator (using GRV-LO-98 proton structure functions [20] and a charm mass of 1.5 GeV) are included in table 3, and are in good agreement with the measured values for all decay channels. A comparison of the  $D^*$  production cross section with predictions using NLO calculations based on the HVQDIS program [21], supplemented by a Peterson [22] fragmentation parametrisation (with  $\epsilon_c = 0.036$  according to [23]) yields  $\sigma_{vis} = 2.55 \text{ nb}$  for charm only, in very good agreement with the LO calculations.

To compare the measurements with previous results,  $\sigma(ep \rightarrow eD^*X)$  was also determined for the same kinematic range as applied in the H1 publication [1], where the only difference

Source of Uncertainty	$D^+$	$D^0$	$D_s^+$	$D^{*+}$
Acceptance	< 2.0			
CJC efficiency	+15.0 -3.0	+10.0 -2.0	+15.0 -3.0	+15.0 -3.0
CJC resolution ( $\pm 10\%$ )	+3.0 -1.5	+0.6 -0.7	+1.8 -3.7	+2.4 -0.5
CST efficiency	$\pm 5.6$	$\pm 3.6$	$\pm 5.4$	$\pm 3.6$
CST resolution ( $\pm 20\%$ )	+2.0 -1.0	+0.4 -0.1	+0.1 -3.6	+1.5 -0.2
vertexing	$\pm 10.0$			
SpaCal calibration ( $\pm 4\%$ )	+3.6 -7.3	+3.4 -8.1	+4.5 -7.8	+4.5 -9.0
signal extraction	+1.7 -0.4	+4.9 -13.4	+1.4 -12.1	+3.7 -3.2
branching ratio	$\pm 6.7$	$\pm 2.3$	$\pm 24.7$	$\pm 2.3$
ISR correction	$\pm 2.6$			
trigger efficiency	$\pm 1.0$			
total systematic error	+21.2 -16.0	+16.5 -19.9	+32.0 -31.8	+20.0 -15.2

Table 4: Relative systematic errors on the inclusive cross sections in % for the different  $D$ -meson decay modes.

was a lower  $p_T(D^*)$  cut of 1.5 GeV. The present analysis yields in that range a value of  $\sigma_{vis} = (5.28 \pm 0.42)$  nb, which agrees with the published H1 result of  $(5.75 \pm 0.35 \pm 0.79)$  nb and also with the LO QCD predictions of 5.53 nb (with GRV-LO 98 proton pdf). Furthermore, the present result is consistent within one  $\sigma$  error with the H1 measurement [24], but it is slightly below the values quoted in [2].

The differential production cross sections were also determined for all decay channels, and results for the  $D^0$  and  $D^+$  channels are shown in fig. 7 and fig. 8 as a function of the various kinematic quantities. The effects of limited detector resolution on the variables are small with respect to the chosen bin sizes and are corrected for using the Monte Carlo simulation. Overlaid in the figures are the predictions of the LO AROMA simulation (dark shaded bands), including a beauty contribution, which was scaled by a factor of 4.3, according to the H1 published values [19]. The beauty contribution itself is indicated separately by light shaded bands. Both the  $p_t(D)$  distribution and the  $\eta(D)$  distribution are quite well described by the LO QCD simulation, even in the forward direction in  $\eta$ . This may be attributed to the improved signal-to-noise ratio achieved with the higher tracking precision even in the forward direction.

### 3.4 Fragmentation Fractions and Isospin Ratios

From the measured cross sections the fragmentation fractions  $f_c$  can be deduced by subtracting the small beauty contribution and then removing the fragmentation dependence  $f_{w.a.}$  from the simulation using the following relation:

$$f(c \rightarrow D) = \frac{\sigma_{vis}(ep \rightarrow eDX) - \sigma_{vis}^{MC}(ep \rightarrow b\bar{b} \rightarrow eDX)}{\frac{\sigma_{vis}^{MC}(ep \rightarrow c\bar{c} \rightarrow eDX)}{f_{w.a.}(c \rightarrow D)}}$$

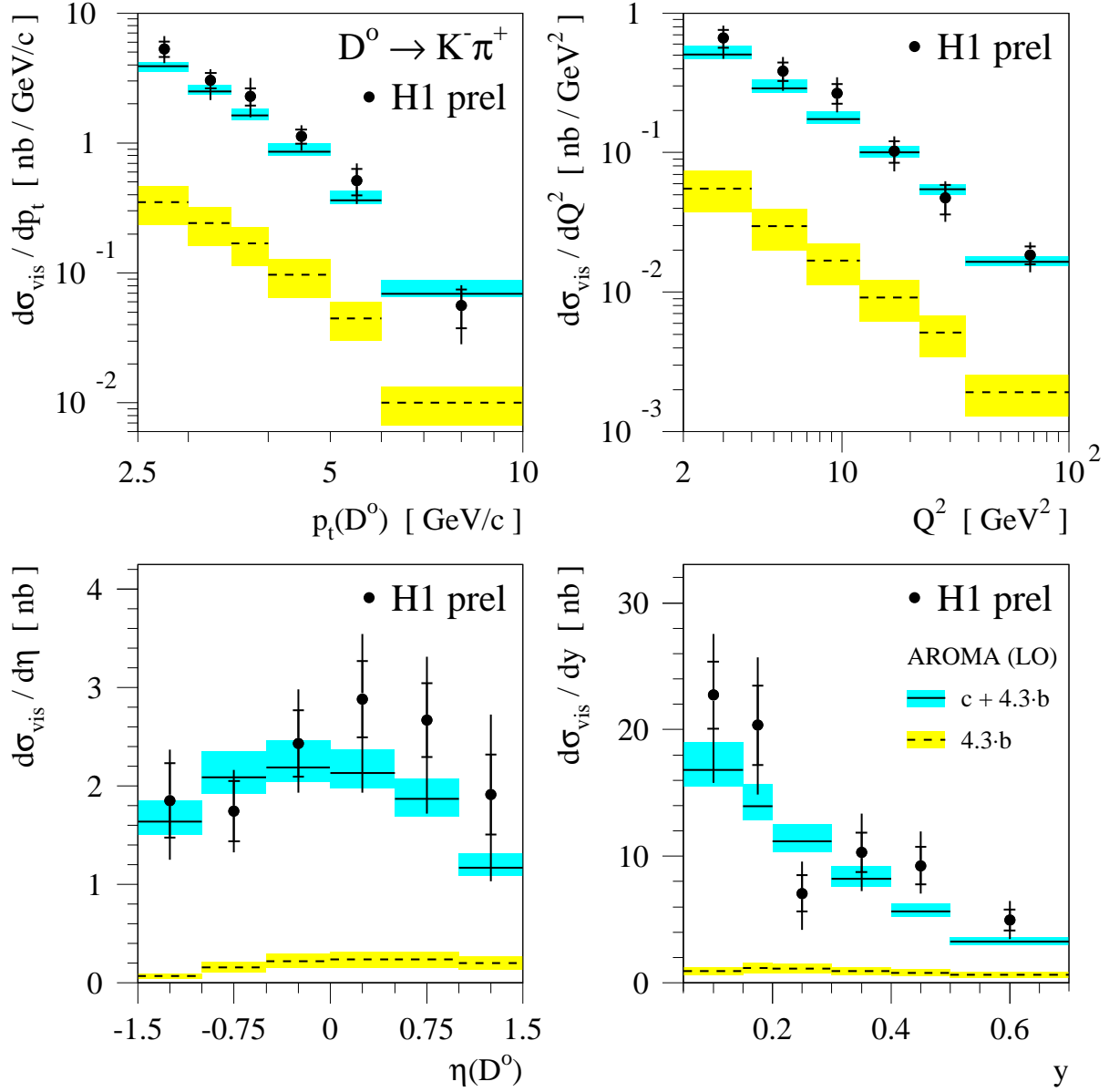


Figure 7: Differential production cross section for  $D^0$  as a function of the  $D^0$  variables (left) and the event variables (right). The dark shaded bands indicate the AROMA MC predictions including a scaled beauty contribution, which is shown separately as light shaded bands.

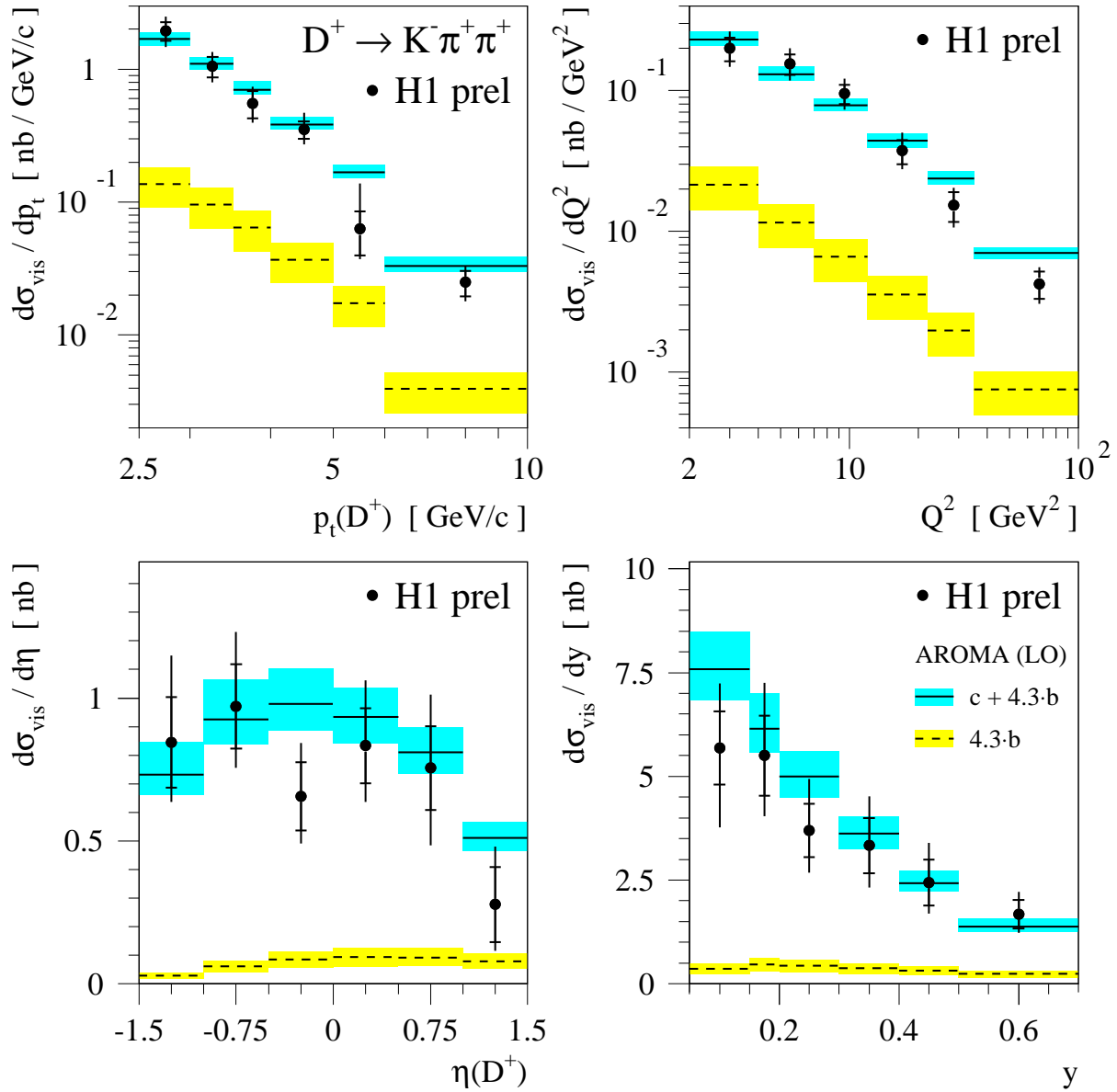


Figure 8: Differential production cross section for  $D^+$  as a function of the  $D^+$  variables (at left) and the event variables (at right). The dark shaded bands indicate the AROMA MC predictions including a scaled beauty contribution, shown separately as light shaded bands.

The resulting values are listed in table 5.

Fragmentation factors	$D^+$	$D^0$	$D_s^+$	$D^{*+}$
$f(c \rightarrow D)$	0.202	0.658	0.156	0.263
stat error	$\pm 0.020$	$\pm 0.054$	$\pm 0.043$	$\pm 0.019$
syst error	+0.045 -0.033	+0.117 -0.142	+0.036 -0.035	+0.056 -0.042
theo error	+0.029 -0.021	+0.086 -0.048	+0.050 -0.046	+0.031 -0.022
$f_{w.a.} = \text{world average}$	$0.232 \pm 0.018$	$0.549 \pm 0.026$	$0.101 \pm 0.027$	$0.235 \pm 0.010$

Table 5: Fragmentation factors deduced from the measured cross sections. The small  $b$  contributions are subtracted. The deduced values compare well with present world average numbers.

Furthermore, the fraction of vector mesons  $P_V$  produced in the fragmentation process can be calculated in different ways based on the extracted fragmentation fractions and using the known branching ratios. The relations are given in the following equations, where  $VM$  denotes the total number of vector mesons and  $PS$  the number of pseudoscalar  $D$  mesons produced in the fragmentation process. The value  $P'_V$  is extracted under the assumption of isospin invariance  $f(c \rightarrow D^{*+}) = f(c \rightarrow D^{*0})$ , and includes directly the  $D^0$  measurements.

$$\begin{aligned}
P_V &= \frac{VM}{PS + VM} \\
&= \frac{f(c \rightarrow D^{*+})}{f(c \rightarrow D^+) + f(c \rightarrow D^{*+}) BR(D^{*+} \rightarrow D^0 \pi^+)} \\
P'_V &= \frac{2 f(c \rightarrow D^{*+})}{f(c \rightarrow D^+) + f(c \rightarrow D^0)}
\end{aligned} \tag{3}$$

Inserting the numbers from table 5, the following results are obtained:  $P_V = (0.693 \pm 0.045 \pm 0.004 \pm 0.009)$  and  $P'_V = (0.613 \pm 0.061 \pm 0.033 \pm 0.008)$ , where the errors are of statistical, systematic and theoretical nature respectively. The theoretical errors include uncertainties due to branching fractions, MC parameter variations and the beauty subtraction. The results compare favourably with the present world average value [25] of  $(0.601 \pm 0.032)$ , which is dominated by measurements performed at  $e^+e^-$  experiments.

In addition, the fragmentation ratios may be determined according to:

$$\begin{aligned}
R_{u/d} &= \frac{f(c \rightarrow D^0) - f(c \rightarrow D^{*+}) BR(D^{*+} \rightarrow D^0 \pi^+)}{f(c \rightarrow D^+) + f(c \rightarrow D^{*+}) BR(D^{*+} \rightarrow D^0 \pi^+)} \\
\gamma_s &= \frac{2 f(c \rightarrow D_s^+)}{f(c \rightarrow D^+) + f(c \rightarrow D^0)}
\end{aligned} \tag{4}$$

The extracted numbers are  $R_{u/d} = (1.26 \pm 0.20 (stat) \pm 0.11 (syst) \pm 0.04 (theory))$ , and  $\gamma_s = (0.36 \pm 0.10 (stat) \pm 0.01 (syst) \pm 0.08 (theory))$ . They too are in agreement with the present world average numbers [25] of  $(1.00 \pm 0.09)$  and  $(0.26 \pm 0.07)$  respectively.

## 4 Conclusions

Production cross sections are measured for the vector  $D^*$  and for the pseudoscalar charmed mesons  $D^0$ ,  $D_S$  and, for the first time at HERA, also  $D^+$  mesons through their decay  $D^+ \rightarrow K^- \pi^+ \pi^+$ . The measurements rely on the proper reconstruction of the vertex separation distance and its error for the  $D$ -meson decays.

The inclusive  $D^*$  production cross sections are, within errors, in agreement with previous measurements and with Monte Carlo predictions based on the leading order AROMA generator program including parton shower modelling.

Differential cross sections are measured for  $D^0$  and  $D^+$  mesons as a function of meson transverse momentum and rapidity, and as a function of the event kinematic variables  $y$  and  $Q^2$ . They are found to be reasonably well described by the LO Monte Carlo predictions.

Based on the measured cross sections, the fragmentation-sensitive parameters  $P_V$ ,  $R_{u/d}$  and  $\gamma_s$  are extracted. They compare favourably with the present world average values, and as such support the hypothesis of universality of charm fragmentation.

## Acknowledgments

We are grateful to the HERA machine group. We thank the engineers and technicians for their work in constructing and now maintaining the H1 detector, our funding agencies for financial support, and the DESY technical staff for continual assistance.

## References

- [1] S. Aid *et al.* (H1 Collaboration), Nucl. Phys. B 545 (1999) 21.
- [2] S. Aid *et al.* (H1 Collaboration), Phys. Lett. B 528 (2002) 199.
- [3] J. Breitweg *et al.* (ZEUS Collaboration), Eur. Phys. C12 (2000) 35
- [4] S. Aid *et al.* (H1 Collaboration), Nucl. Phys. B 472 (1996) 32.
- [5] S. Frixione *et al.*, J. Phys. G 27 (2001) 1111.
- [6] P. Nason, G. Ridolfi *et al.* in LHC workshop on Standard Model Physics e-Print Archive: hep-ph/0003142, (2000).
- [7] I. Abt *et al.* (H1 Collaboration) Nucl. Instr. Meth. A 386 (1997) 310, and *ibid.* 348.
- [8] J. Bürger *et al.*, Nucl. Instr. Meth. A 279 (1989) 217.
- [9] I. Abt *et al.* (H1 Collaboration), Phys. Lett. B 328 (1994) 176.
- [10] D. Pitzl *et al.* (H1 Collaboration) Nucl. Instr. Meth. A 454 (2000) 334.
- [11] K. Müller *et al.*, Nucl. Instr. Meth. A 312 (1992) 457.

- [12] R. D. Appuhn *et al.* (H1 SpaCal group), Nucl. Instrum. Meth. A 386 (1997) 397.
- [13] H1 Collaboration, Technical proposal for the upgrade of the backward region of the H1 detector, DESY internal report PRC-93/02.
- [14] S. Aid *et al.* (H1 Collaboration), Nucl. Phys. B 497 (1997) 3.
- [15] U. Bassler and G. Bernardi, Nucl. Instrum. Meth. A 361 (1995) 197.
- [16] G. Feldmann *et al.*, Phys. Rev. Lett. 38 (1977) 1313.
- [17] G. Ingelman, J. Rathsman and G. A. Schuler, Comput. Phys. Commun. 101 (1997) 135.
- [18] T. Sjöstrand, CERN-TH-6488 (1992), Comp. Phys. Comm. 82 (1994) 74.
- [19] S. Aid *et al.* (H1 Collaboration), Phys. Lett. B 467 (1999) 156.
- [20] M. Glück, E. Reya and A. Vogt, Eur. Phys. J. C 5 (1998) 461.
- [21] B. W. Harris and J. Smith, Phys. Rev. D 57 (1998) 2806.
- [22] C. Peterson, D. Schlatter, I. Schmitt, and P. M. Zerwas, Phys. Rev. D 27 (1983) 105.
- [23] P. Nason and C. Oleari, preprint CERN-TH/98-339 (1998).
- [24] S. Aid *et al.* (H1 Collaboration), Phys. Lett. B 520 (2001) 191.
- [25] L. Gladilin, e-Print Archive: hep-ex/9912064, (1999).